The Journal of Chemical Physics

Identification of the Jahn–Teller active trichlorosiloxy ($SiCl_3O$) free radical in the gas phase

Cite as: J. Chem. Phys. **152**, 194303 (2020); https://doi.org/10.1063/5.0009223
Submitted: 29 March 2020 . Accepted: 27 April 2020 . Published Online: 19 May 2020

Tony C. Smith, and Dennis J. Clouthier

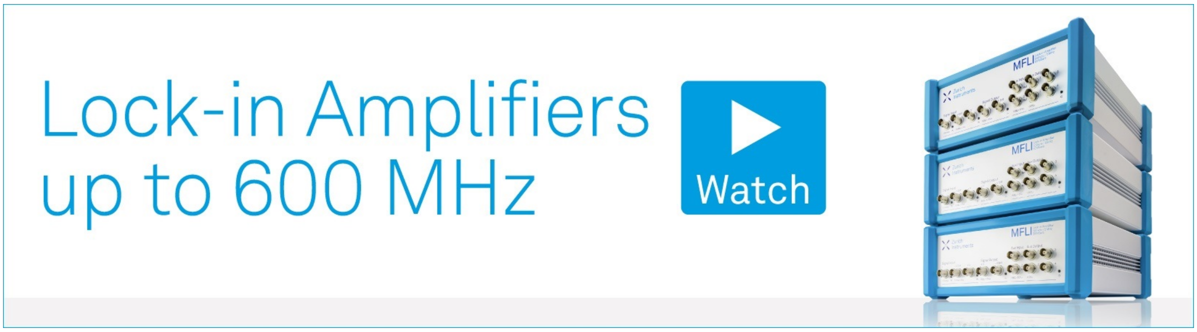

AIP Publishing

Identification of the Jahn–Teller active trichlorosiloxy ($SiCl_3O$) free radical in the gas phase

Cite as: J. Chem. Phys. **152**, 194303 (2020); doi: 10.1063/5.0009223
Submitted: 29 March 2020 • Accepted: 27 April 2020 •
Published Online: 19 May 2020

Tony C. Smith and Dennis J. Clouthier[a]

AFFILIATIONS

Ideal Vacuum Products, LLC, 5910 Midway Park Blvd. NE, Albuquerque, New Mexico 87109, USA

[a] **Author to whom correspondence should be addressed:** djc@idealvac.com

ABSTRACT

The $\tilde{A}^2A_1$–$\tilde{X}^2E$ electronic transition of the jet-cooled trichlorosiloxy ($SiCl_3O$) free radical has been observed for the first time in the 650–590 nm region by laser induced fluorescence (LIF) detection. The radical was produced by a pulsed electric discharge through a mixture of silicon tetrachloride and oxygen in high pressure argon at the exit of a pulsed molecular beam valve. The LIF spectrum shows low frequency intervals, which we assign as activity in the normally forbidden degenerate v_5' and v_6' modes, indicative of a significant Jahn–Teller effect in the ground state. Single vibronic level emission spectra show level dependent spin–orbit splittings in the ground state and Jahn–Teller predictable variations depending on which upper state level is pumped. The measured lower state energy levels have been fitted to a Jahn–Teller model that simultaneously includes spin–orbit coupling and linear and quadratic multimode coupling. In $SiCl_3O$, the Jahn–Teller interaction predominates over spin–orbit effects.

I. INTRODUCTION

Silanes (SiX_4) and siloxanes (X_3Si–O–SiX_3) are important precursor compounds in the industrial production of silicon thin films for semiconductors and high purity silica for the optical fibers used in telecommunications. In the process of precursor degradation, either by high temperature reactions or in plasmas, it has been shown theoretically[1,2] that a large variety of reactive intermediates are produced although few of these have been identified chemically or spectroscopically. In particular, one class of such species, the siloxy free radicals (SiX_3O), is unknown, despite its direct relevance to several industrial processes.

There are many motivations for spectroscopic studies of silicon-based reactive systems, due to the pivotal role they play in semiconductor growth processes. Many such species have been postulated, but few have actually been identified or characterized. For example, $Si_xH_yO_z$ molecules are thought to be intermediates in the oxidation of SiH_4 and play an important role in the formation of Si, SiO, and SiO_2 thin films and nanoparticles.[2] As pointed out by Hitchman and Jensen[3] in their review of chemical vapor deposition (CVD) processes, "despite the increased use of diagnostic procedures for monitoring CVD reactions, still relatively little is known about the nature of gas phase intermediates in most deposition processes, and even less is known about the kinetic parameters for the formation and consumption of those intermediates." It is, therefore, important to establish sensitive methods for detecting and characterizing reactive species to aid in experimental and theoretical programs aimed at optimizing semiconductor growth processes. Such methods are most likely to be spectroscopic in nature, and future studies of the transient intermediates involved in semiconductor growth processes will rely on a well-established database of molecular constants, transition frequencies, transition intensities, and photophysical parameters.

Of particular interest in the present work is the high temperature reaction of $SiCl_4$ with O_2, an industrially important process that leads to the production of silicon dioxide aerosols and high-purity silica for the optical fibers used in telecommunications. The reaction appears to be exceedingly complex, especially in the 800–1000 °C range, generating a multitude of chlorosiloxanes with the general formula $Si_xO_yCl_z$, which have been identified by mass spectrometry[4] and limited matrix isolation studies.[5,6] Recent laser-induced fluorescence studies of the products of electric discharges in $SiCl_4$ + O_2 mixtures in our laboratory sparked our interest in the chlorosiloxy radicals ($SiCl_3O$) as possible intermediates in silicon tetrachloride oxidation processes. The oxidation of silane is also of considerable interest, both as a fundamental model system, which is still poorly understood,[2] and as a method for the production of SiO_2 thin films. Low-pressure chemical vapor deposition using $SiH_4/O_2/N_2$ gas mixtures has been studied, and the film growth is thought to be originated by an unknown SiO_xH_y intermediate in the gas phase.[2] Whether the SiH_3O radicals participate in such reactions is unknown. In a similar fashion, fluorine-containing gases, often with added oxygen, are used in the plasma etching of Si, SiO_2, and SiN materials, and SiF_3O radicals may be formed under such conditions.[7]

In sharp contrast to the wealth of information in the literature about Jahn–Teller active methoxy radicals,[8] virtually nothing is known about the corresponding small siloxy (SiX_3O) radicals. Neutralization reionization mass spectrometry experiments[9] have shown that SiH_3O can be made from the corresponding cation and that it is stable during the μs time scale of the experiment. The SiF_3O radical has been detected in electron spin resonance experiments,[10] and the intermediacy of the $SiCl_3O$ radical has been postulated to explain the results of gas phase FTIR studies of trichlorosilyl radical reactions.[11] None of these species have been detected or studied in the gas phase by spectroscopic techniques.

By comparison with the methoxy radicals, we can anticipate that the ground state of the siloxy free radicals will be ^2E. However, the Jahn–Teller distortion will split this into a $^2A'$ and a $^2A''$ component. In addition, these states will have spin–orbit splittings whose magnitude will depend on the extent of the Jahn–Teller quenching. The upper state will be $^2A_1$ and does not, therefore, have any Jahn–Teller complications. The extent of activity of the non-totally symmetric (e) vibrational modes (ν_4' - ν_6') in the absorption [or laser induced fluorescence (LIF)] spectra depends again on the extent of the Jahn–Teller effect in the lower state. The presence of bands involving the e modes in LIF or emission spectra would be characteristic of the siloxy radicals with a significant Jahn–Teller effect in the ground electronic state.

In the present work, we have conclusively identified the laser-induced fluorescence spectrum of the jet-cooled $SiCl_3O$ free radical in the gas phase. Analysis of single vibronic level (SVL) emission spectra has shown that the ground state is subject to a significant Jahn–Teller effect, which is evident in the pronounced activity of the normally forbidden degenerate ν_5' and ν_6' modes. The measured lower state vibronic energy levels have been fitted with a Jahn–Teller model that includes spin–orbit coupling and linear and quadratic multimode coupling. The resulting parameters have been used to simulate SVL emission spectra, which are found to agree satisfactorily with experiment, validating the analysis.

II. EXPERIMENT

It was found that a new LIF spectrum attributable to the $SiCl_3O$ radical could be generated either using a precursor mixture of $SiCl_4$ and oxygen (60 Torr of each) in high pressure (120 psi) argon or by seeding the room temperature vapor pressure (~7 Torr) of hexachlorodisiloxane ($Cl_3SiOSiCl_3$, Gelest, 90%) in 50 psi of argon. As described in detail elsewhere,[12,13] a pulsed molecular beam valve (General Valve, series 9) injected the precursor mixture into a flow channel where an electric discharge between two stainless steel ring electrodes fragmented the precursor, producing the species of interest and a variety of other products. The reactive intermediates were rotationally and vibrationally cooled by free jet expansion into vacuum at the exit of the pulsed discharge apparatus. A 1.0 cm long reheat tube[14] added to the end of the discharge apparatus increased production of the radicals and suppressed the background glow from excited argon atoms.

Low resolution (0.1 cm^{-1}) LIF spectra were recorded using a neodymium:yttrium aluminum garnet (Nd:YAG) pumped dye laser (Lumonics HD-500) excitation source. The fluorescence was collected using a lens and focused through appropriate longwave pass filters and onto the photocathode of a photomultiplier tube (RCA C31034A). The spectra were calibrated with optogalvanic lines from various argon- and neon-filled hollow cathode lamps. The laser-induced fluorescence and calibration spectra were digitized and recorded simultaneously on a homebuilt computerized data acquisition system.

For emission spectroscopy, the band maxima of features in the LIF spectrum were excited by the dye laser, and the resulting fluorescence was imaged with $f/4$ optics onto the entrance slit of a 0.5 m scanning monochromator (Spex 500M). The pulsed fluorescence signals were detected with a gated CCD camera (Andor iStar 320T) and recorded digitally. The emission spectra were calibrated to an estimated accuracy of ±1 cm^{-1} using emission lines from an argon filled hollow cathode lamp. A 1200 line/mm grating blazed at 750 nm was employed in this work, which gave a band pass of 29.9 nm with an 18 mm effective active area on the CCD.

III. RESULTS AND ANALYSIS

A. *Ab initio* calculations

We have carried out a series of modest level *ab initio* calculations to predict the properties of the ground and excited states of the $SiCl_3O$ free radical using the Gaussian 09 program package.[15] The ^2E C_{3v} ground state is subject to the Jahn–Teller distortion, and by starting with a slightly lower symmetry geometry, we were able to converge on a $^2A'$ ground state with all positive frequencies using density functional (B3LYP)[16,17] and second order Moller–Plesset (MP2) theory using a triple zeta basis set with added d orbital polarization functions (6-311G*). The ground state has an $\ldots a_1^2\, e^3$ electron configuration (C_{3v} notation), with the geometry distortion as shown in Fig. 1. The unpaired electron is almost completely localized on the oxygen atom. The geometric parameters, vibrational frequencies, and energies are reported in Table I.

The $\tilde{A}^2A_1$ excited state involves the promotion of an a_1 second highest occupied molecular orbital (SHOMO) electron to the highest occupied molecular orbital (HOMO) of e symmetry. This state is not orbitally degenerate and, therefore, not subject to the Jahn–Teller distortion, so the symmetry is rigorously C_{3v}. The electron promotion involves a migration of unpaired electron density from the oxygen atom to the chlorine atoms although the majority

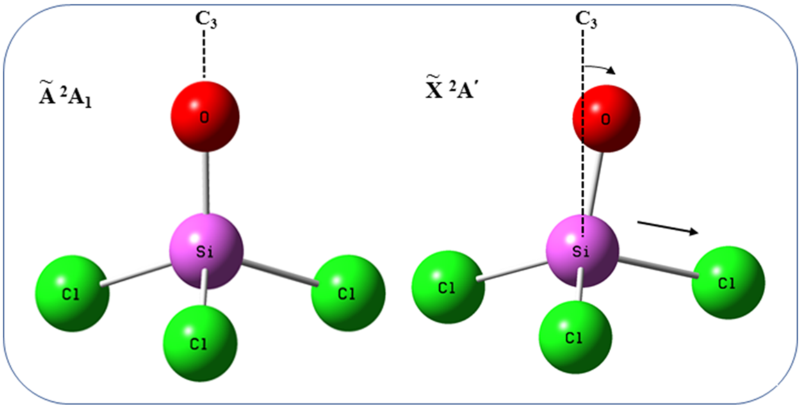

FIG. 1. The molecular structures of the $SiCl_3O$ free radical in the electronic excited and ground states. The distortion of the latter has been greatly exaggerated to show the Jahn–Teller symmetry breaking, which involves an elongation of one of the Si–Cl bonds and a rotation of the Si–O moiety off the C_3 axis.

remains on the oxygen. The calculated properties of the excited state are summarized in Table I.

The calculations indicate that the first electronic transition of $SiCl_3O$ free radical should occur in the visible spectrum around 15 000 cm^{-1} (~670 nm) and that the ground state is subject to a substantial Jahn–Teller distortion. On electronic excitation, only the ν_5 and ν_6 vibrational frequencies change significantly, and the geometric parameters, with the exception of a ~0.04 Å diminution of the Si–O bond length, are largely unaffected.

B. The Jahn–Teller effect

In this section, we summarize important aspects of the Jahn–Teller effect that are relevant to our analysis of the $SiCl_4 + O_2$ spectrum. These come from the literature following the general discussion of Herzberg[18] and the more detailed experimental and theoretical studies by Barckholtz and co-workers.[8] In a molecule with degenerate modes of vibration, there is a vibrational angular momentum in the direction of the symmetry axis characterized by the quantum number $l_i = v_i, v_i - 2, \ldots, 1$ or 0. The levels of different l_i and the same v_i would be degenerate at the lowest level of approximation. In nondegenerate electronic states, these levels do show small splittings due to anharmonicity. However, in degenerate electronic states, the vibrational angular momentum is coupled with the electronic orbital angular momentum to form a resultant *vibronic* angular momentum, which generally causes a substantial splitting of the degenerate vibrational levels. In linear (and bent molecules with less than a threefold axis of symmetry), this type of vibronic interaction is termed the Renner–Teller effect. In nonlinear molecules with a threefold or greater symmetry axis and a degenerate electronic state, the vibronic coupling is termed the Jahn–Teller effect.

The Jahn–Teller theorem proves that any state with a degenerate electronic wave function is unstable in the most symmetric

TABLE I. The *ab initio* parameters (MP2, with B3LYP in parentheses, the basis set is 6-311G* in both cases) for ${}^{28}Si^{35}Cl_3{}^{16}O$. Quantities without explicit units are in cm^{-1}.

Parameter	$\tilde{X}^2A'$	$\tilde{A}^2A_1$
r(Si–Cl) (Å)	2.017/2.014[a] (2.039/2.042)	2.014 (2.053)
r(Si–O) (Å)	1.666 (1.653)	1.632 (1.605)
<(Cl–Si–O) (deg)	110.6/103.7 (111.8/101.2)	108.9 (110.1)
<(Cl–Si–Cl) (deg)	111.5/103.7 (111.5/108.8)	110.0 (108.9)
ω_1 (Si–O symm. stretch, a_1)[b]	904 (872)	899 (903)
ω_2 (Si–Cl symm. stretch, a_1)	474 (443)	480 (422)
ω_3 (Si–Cl_3 umbrella, a_1)	245 (223)	255 (236)
ω_4 (Si–Cl asymm. stretch, e)	646/653 (595/604)	653 (562)
ω_5 (Si–Cl_3 rock, e)	251/258 (234/240)	305 (293)
ω_6 (Si–Cl_2 scissors, e)	100/178 (116/162)	179 (167)
T_0	. . .	16 468 (14 130)

[a] In the Jahn–Teller distorted ground state, the Si–Cl bond lengths and angles are not all equivalent. In each case, the first entry is the value for the two equivalent parameters and the second for the unique value.

[b] The symmetry labels apply strictly to the C_{3v} symmetry. In the Jahn–Teller distorted ground state, the "e" modes are not quite degenerate, so two distinct frequencies are given.

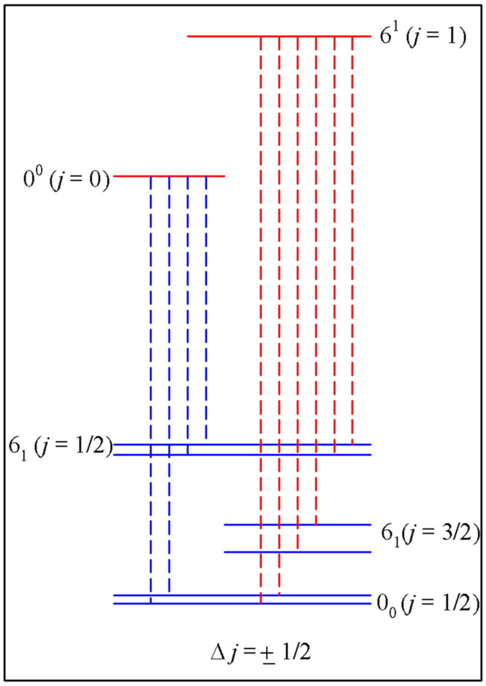

FIG. 2. Schematic energy levels for the $SiCl_3O$ free radical, showing the allowed transitions.

conformation and will exhibit a spontaneous symmetry breaking that lowers the overall energy. The vibronic interaction splits the degeneracy of the vibrational levels so that there will be as many different vibronic levels as there are vibronic species for each vibrational level. The vibronic interaction compromises the goodness of the electronic orbital angular momentum quantum number $\Lambda = \pm 1$ and the previously defined vibrational angular momentum quantum numbers l_i leading to the definition of a new first order Jahn–Teller quantum number, which, for molecules of C_{3v} symmetry, is

$$j = l + \Lambda/2 = 1/2, 3/2, 5/2, 7/2, \text{ etc.} \tag{1}$$

The states with $j = 3/2, 9/2, \ldots$ transform as a_1 or a_2, while all others, $j = 1/2, 5/2, 7/2, 11/2, \ldots$, transform as e. In a nondegenerate state, for example, the $^2A_1$ excited state of the $SiCl_3O$ radical, $j = l$. The relevant vibronic selection rule is then $\Delta j = \pm 1/2$.

The presence of an unpaired electron further complicates the situation. In an orbitally nondegenerate state, such as the $\tilde{A}^2A_1$ state of $SiCl_3O$, spin–orbit coupling is usually very small, and its effect on the vibronic levels can be neglected. However, in orbitally degenerate states, spin–orbit coupling can be substantial, similar to that for the Π, Δ . . . electronic states of linear molecules. For large spin–orbit coupling, the Jahn–Teller instability is quenched, whereas small spin–orbit coupling has the effect of splitting some of the vibronic states into two spin–orbit components. The conventional notation is to designate the vibrational level, such as 5_1, and add a superscript + or − indicating whether the level is the upper or lower spin component, respectively, along with the j value in parentheses.

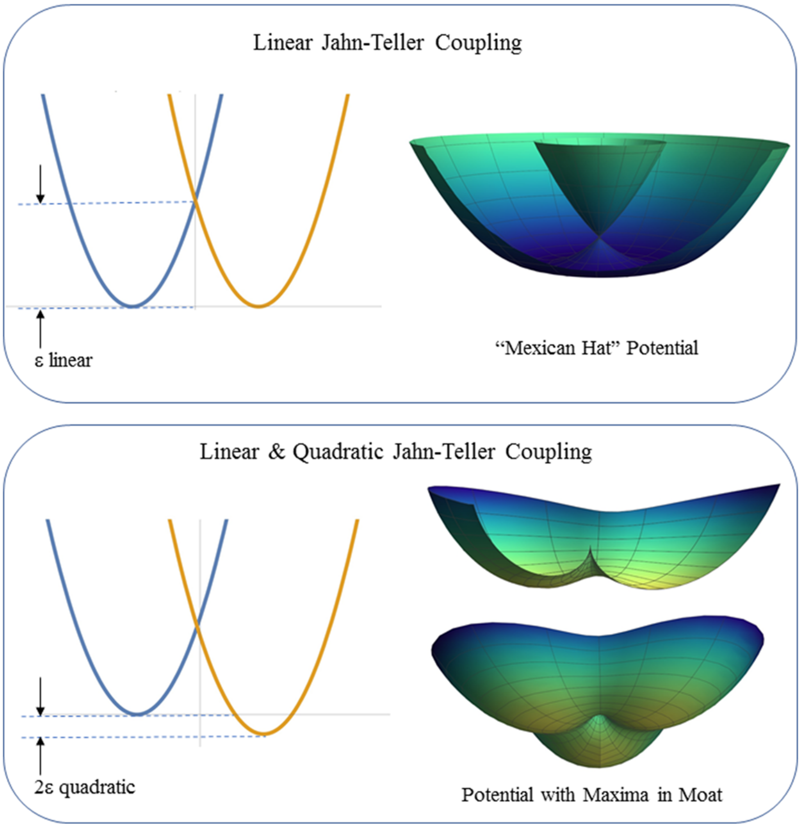

FIG. 3. Schematic potential energy surfaces (PES) for the Jahn–Teller distorted C_{3v} ground state of a species like the $SiCl_3O$ free radical. The top panel shows the PES resulting from the linear Jahn–Teller coupling, which produces a "Mexican hat" potential with a circular moat. The bottom panel shows the effect of linear plus quadratic Jahn–Teller coupling, which creates local minima and maxima around the moat.

Thus, $5_1^+(j = 1/2)$ denotes the upper spin–orbit component of the $j = 1/2$ level of $v_5'' = 1$. It is important to note that the eigenvectors are actually a linear combination of basis functions in the solution of the Jahn–Teller problem and this notation, where appropriate, only designates the leading term in the expansion. If the combining electronic states have the same spin multiplicity, then the $\Delta S = 0$ selection rule is satisfied, and in $SiCl_3O$, transitions can occur from an upper state vibronic level to both spin–orbit components of a lower state vibronic level as long as the $\Delta j = \pm 1/2$ selection rule is satisfied. The spin–orbit coupling in the Jahn–Teller active state is quantified by the spin–orbit coupling constant $a\zeta_e$, where the dimensionless ζ_e is the projection of the electronic orbital angular momentum on the symmetry axis and a (cm^{-1}) is an approximate measure of the strength of the interaction of the unpaired electron with the individual nucleus.

With this background, we show in Fig. 2 a schematic of a few of the relevant vibronic energy levels for the $\tilde{A}^2A_1$ and $\tilde{X}^2E$ electronic states of the $SiCl_3O$ free radical. The v_6 vibration is doubly degenerate, and the Jahn–Teller and spin–orbit interactions in the ground state lead to four levels (j = ½ and 3/2) with the vibrational label 6_1. Due to the Jahn–Teller coupling, the ground state 0_0 level is actually an admixture of the vibrational basis functions of the degenerate modes, so both the excitation and emission spectra will exhibit features due to the Jahn–Teller active modes, subject only to the $\Delta j = \pm 1/2$ restriction. Cold band absorption or LIF spectra from 0_0 will then involve transitions to the totally symmetric levels (0_0, 1_1, 2_1, 3_1) with $j = 0$ and to levels involving the degenerate modes with $j = 1$ or 0. Single vibronic level emission spectroscopy is the key to understanding the lower state Jahn–Teller problem. As shown in Fig. 2, emission from the 0^0 level ($j = 0$) can only terminate on j = ½ levels, accessing only half of the 6_1 vibrational states. However, emission from the 6^1 level ($j = 1$) is allowed to both j = ½ and j = 3/2 states, so a comparison of the two types of emission spectra can be used to differentiate between these levels. In addition, observation of these differences can provide confirmation of LIF assignments.

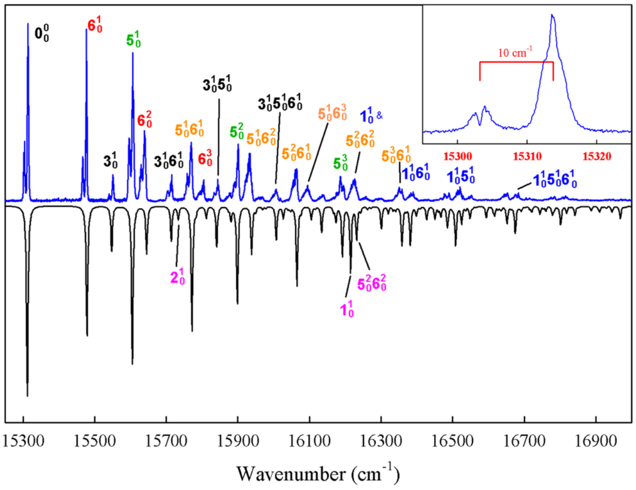

FIG. 4. The $\tilde{A}^2A_1$–$\tilde{X}^2E$ LIF spectrum of the jet-cooled $SiCl_3O$ free radical with vibronic assignments. The inset shows the spin splitting of the 0_0^0 band. The negative going spectrum is a Franck–Condon simulation of the expected absorption spectrum based on the *ab initio* vibrational frequencies and Cartesian displacement coordinates of the combining states (Table I). The simulation predicts a weak 2_0^1 band that is clearly not evident in the experimental spectrum.

Finally, it is necessary to discuss the potential energy surfaces and the parameters that are used to define the Jahn–Teller coupling. The usual treatment of the problem results in a potential that can be approximated as the sum of a linear and a quadratic term.[8] The linear Jahn–Teller coupling distorts the molecule of nominally C_{3v} symmetry, so that the potential for a single active mode has a global minimum at the bottom of the moat, as shown in Fig. 3, and is characterized by a dimensionless linear Jahn–Teller coupling constant D_i for the ith mode. The previously defined quantum number $j = l + \Lambda/2$ is only strictly conserved for linear coupling. Quadratic coupling modifies the moat, so that it contains maxima and minima (3 in C_{3v} symmetry, see Fig. 3), and the extra stabilization is characterized by the dimensionless quadratic coupling constant K_i. In practice, one can use the Spin-Orbit Coupling and Jahn–Teller (SOCJT) program of Barckholtz and Miller[19] to fit the observed

TABLE II. Approximate band centers (cm^{-1}) and assignments [originating from the lower or (-) spin–orbit component in the ground state] of the features in the LIF spectrum of the $SiCl_3O$ free radical. The feature quoted in parentheses is the band center of the less intense spin–orbit component (where resolved), which is the transition from the upper or (+) level.

Band center (cm^{-1})	Assignment	Comment
15 313.7 (15 303.2)	0_0^0	Spin–orbit = 10.5
15 477.3 (15 467.0)	6_0^1	$\nu_6' = 163.6$
15 551.0 (15 541.0)	3_0^1	$\nu_3' = 237.3$
15 606.4 (15 597.1)	5_0^1	$\nu_5' = 292.7$
15 639.2 (15 630.0)	6_0^2	$6_0^1 + 161.9$
15 715.3 (15 704.7)	$3_0^1 6_0^1$	$6_0^1 + 238$
15 769.0 (16 758.4)	$5_0^1 6_0^1$	$6_0^1 + 291.7$
15 804.3 (15 794.6)	6_0^3	$6_0^2 + 165.1$
15 843.7 (15 833.7)	$3_0^1 5_0^1$	$3_0^1 + 292.7$
15 901.1 (15 891.5)	5_0^2	$5_0^1 + 294.7$
15 934.1	$5_0^1 6_0^2$	$6_0^2 + 294.9$
16 006.6	$3_0^1 5_0^1 6_0^1$	$3_0^1 5_0^1 + 162.9$
16 063.3	$5_0^2 6_0^1$	$5_0^2 + 162.2$
16 094.7	$5_0^1 6_0^3$	$6_0^3 + 290.4$
16 186.3	5_0^3	$5_0^2 + 285.2$
16 226.2	1_0^1 and $5_0^2 6_0^2$	$\nu_1' = 912.6$
16 350.3?	$5_0^3 6_0^1$	$5_0^3 + 164.0$
16 389.6?	$1_0^1 6_0^1$	$6_0^1 + 912.3$
16 490.0	5_0^4	$5_0^3 + 303.7$
16 520.1	$1_0^1 5_0^1$	$5_0^1 + 913.7$
16 552.6	$1_0^1 6_0^2$	$6_0^2 + 913.4$
16 653.8	$5_0^4 6_0^1$	$5_0^4 + 163.8$
16 683.3	$1_0^1 5_0^1 6_0^1$	$5_0^1 6_0^1 + 914.3$
16 784.6	5_0^5	$5_0^4 + 294.6$
16 816.0	$1_0^1 5_0^2$	$5_0^2 + 914.9$

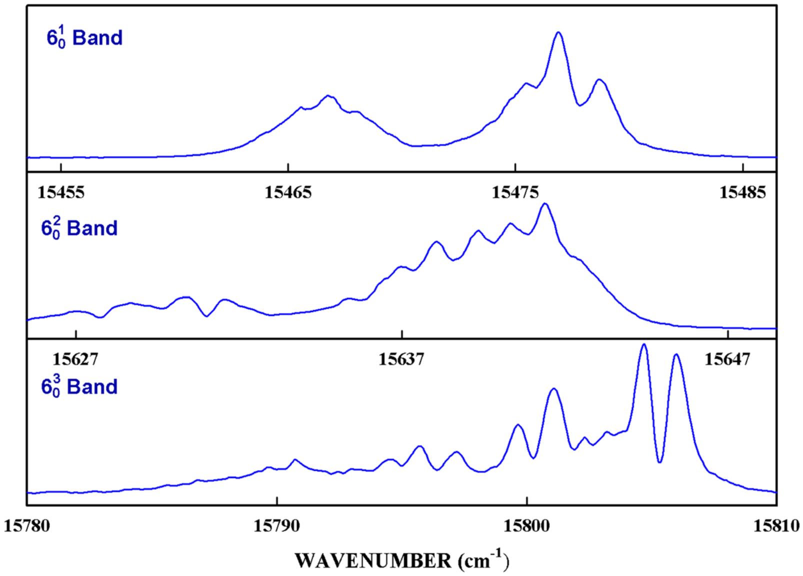

FIG. 5. The experimentally observed rotational profiles of the 6_0^1, 6_0^2, and 6_0^3 LIF bands of the $SiCl_3O$ free radical.

vibronic energy levels of a C_{3v} Jahn–Teller active state to obtain the Jahn–Teller and spin–orbit coupling parameters and validate the analysis by simulation of the observed absorption and emission spectra.

C. LIF and emission spectra

An intense LIF spectrum with an onset at 15 300 cm^{-1} and extending to 16 900 cm^{-1}, illustrated in Fig. 4, was discovered using the $SiCl_4 + O_2$ precursor mixture. It was, subsequently, shown that exactly the same spectrum could be obtained using hexachlorodisiloxane ($Cl_3Si–O–SiCl_3$) as the starting material. The spectrum commences with a strong 0–0 band at 15 313.5 cm^{-1}, nearby strong bands +163.5 cm^{-1} and +292.9 cm^{-1} higher in energy, and then a wealth of weaker bands out to 16 900 cm^{-1}. The strong bands show a distinct splitting with a weaker satellite 10–15 cm^{-1} to lower energy, as shown in the inset of Fig. 4.

In the absence of Jahn–Teller distortions, the absorption spectrum for a $^2A_1$–^2E electronic transition should consist of vibronic transitions involving only the totally symmetric vibrational modes. It is readily apparent from the low frequency intervals in the spectrum (experiments in which the expansion conditions were changed show these are cold bands) that the e' modes must be involved, as anticipated for a Jahn–Teller active ground state. In fact, the *ab initio* vibrational frequencies (Table I, $\omega_6' \sim 175$ cm^{-1} and $\omega_5' \sim 300$ cm^{-1}) immediately suggest assignments of 6_0^1 (+163.5 cm^{-1})

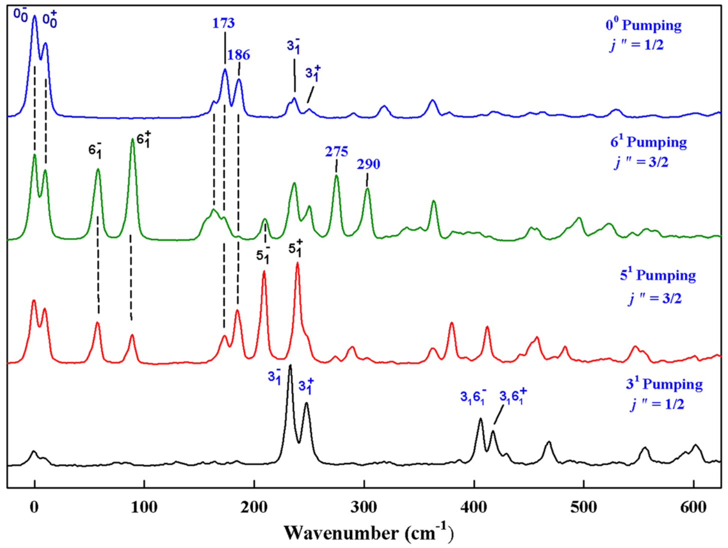

FIG. 6. A comparison of the single vibronic level emission spectra of the $SiCl_3O$ free radical for laser excitation of the LIF 0_0^0, 6_0^1, 5_0^1, and 3_0^1 bands (stronger spin–orbit component in each case). The assignments and lower state *j* values for a few key features in the spectra are given. Vertical dashed lines link features with the same lower state. The spectra are plotted as displacement from the laser excitation wave number (cm^{-1}), giving a direct measure of the relative ground state energy for each transition.

and 5^1_0 (+292.9 cm^{-1}) for the first two strong bands above the 0–0 band. A much weaker band at +238 cm^{-1} (calc. = 252 cm^{-1}) is identified as 3^1_0. The prominence of the 5^1_0 and 6^1_0 bands in the spectrum suggests that the ground state Jahn–Teller effect is substantial. The pattern of bands repeats with fairly harmonic intervals throughout the spectrum so that most features can be assigned as involving v'_3, v'_5, and v'_6, until a weak peak at 16 389 cm^{-1}, +1076 cm^{-1} above the 0–0 band. This interval is too large to be a ground state vibrational fundamental (see Table I) but can be assigned as $v'_1 + v'_6$ (*ab initio* = 1070–1078 cm^{-1}). Subtracting the experimental v'_6 = 163.6 cm^{-1} yields 1^1_0 = 16 225.4 cm^{-1}, coincident with a broad observed band we assigned as $5^1_0 6^1_0$. It is likely that both vibronic transitions are buried under the profile of this band, and we have made this assignment in Fig. 4. The measured band centers, spin–orbit splittings, and assignments of the LIF spectrum are summarized in Table II.

In the latter stages of the analysis, we attempted to simulate the LIF spectrum by calculating the Franck–Condon (FC) factors for all possible transitions in the harmonic approximation, using the program previously described.[20,21] The input was the B3LYP/6-311G* geometries, vibrational frequencies (see Table I), and mass-weighted Cartesian displacement coordinates from the *ab initio* output. If we constrain both states to have C_{3v} symmetry, we obtain a very simple predicted absorption spectrum, which only involves the totally symmetric modes, as anticipated from the vibrational selection rules, with prominent 3^1_0, 1^1_0, and 1^2_0 transitions. If we allow the lower state to undergo the Jahn–Teller distortion to the geometry shown in Table I, the resulting spectrum, shown as the downward-going trace in Fig. 4, is astonishingly similar to the experiment, clearly establishing that the species responsible for the observed LIF spectrum is the $SiCl_3O$ free radical. Of course, the simulation does not include spin–orbit effects, so the small splittings observed experimentally are not evident, which also provides confirmation that we are dealing with a species with an unpaired electron. The FC simulation also provided strong evidence for the validity of our initial vibronic assignments of the LIF spectrum, including the overlap of 1^1_0 and $5^2_0 6^2_0$ and the absence of activity in v'_2 and v'_4.

The rotational contours of the 6^1_0, 6^2_0, and 6^3_0 bands are shown in Fig. 5, illustrating the complexity of the higher bands in the spectrum. For a molecule as heavy as $SiCl_3O$, we would not expect any resolvable rotational structure at our resolution of 0.1 cm^{-1}, even at our estimated rotational temperature of 15 K, and this is evidently the case. The three chlorine atoms (^{35}Cl = 75.77%, ^{37}Cl = 24.23%) should lead to more and more isotopic complications in the band contours with additional quanta of v'_6 (the Si–Cl_2 scissors mode), whose *ab initio* fundamental frequency we find to be affected by 1–4 cm^{-1} depending on which chlorine isotopologue one calculates. These changes in the band contour made it difficult to obtain precise band positions and vibrational intervals from the LIF spectra.

The SVL emission spectra obtained from pumping the 0^0_0, 6^1_0, 5^1_0, and 3^1_0 bands in the $SiCl_3O$ LIF spectrum are compared in Fig. 6. It is immediately apparent that the 0^0 and 6^1 emission spectra exhibit the behavior predicted in Fig. 2, with new transitions down to 6_1 (j = 3/2) evident in the latter. A similar pattern is found in the 5^1 emission with transitions down to the 5_1 (j = 3/2) levels. In sharp contrast, the 3^1 emission spectrum is dominated by an intense transition to a level at 233 cm^{-1}, which is readily assigned as 3_1 based on the *ab initio* vibrational frequencies (Table I) of 245 cm^{-1} and 223 cm^{-1}. There is also a prominent feature (not shown) in the 0–0 band spectrum at a displacement of 894 cm^{-1} with a spin splitting of 11 cm^{-1}, which we assign as 1^0_1 (*ab initio* v''_6 = 904 cm^{-1} and 872 cm^{-1}). It is very clear that the observed rotational contours, isotopic splittings, vibrational intervals, Jahn–Teller splittings, and very good agreement between the observed and calculated Franck–Condon profiles of the LIF spectra are entirely consistent with our assignment of the carrier as the $SiCl_3O$ free radical.

D. Jahn–Teller analysis of the ground state vibronic energy levels

The emission spectra (Fig. 6) provide us with the most information on the ground state vibronic energy levels of the $SiCl_3O$ free radical. We have used the SOCJT program[19] to fit our data: the input

TABLE III. Energies (cm^{-1}), assignments, quantum numbers, and Obs–Calc residuals (cm^{-1}) for the ground state vibronic energy levels of the $SiCl_3O$ free radical.

Energy (Assign.)	j	n_j	Σ	Obs–Calc
0 (0^-_0)	0.5	1	0.5	0.0
10 (0^+_0)	0.5	1	−0.5	6.6
58 (6^-_1)	1.5	1	−0.5	9.4
89 (6^+_1)	1.5	2	−0.5	−1.3
155	0.5	2	−0.5	1.7
162	0.5	2	0.5	1.3
173	0.5	3	0.5	6.3
184	0.5	3	−0.5	3.5
210 (5^-_1)	1.5	3	−0.5	3.3
239 (5^+_1)	1.5	4	−0.5	−2.6
245	0.5	4	−0.5	−3.4
250	0.5	4	0.5	−2.6
275	1.5	5	−0.5	3.3
290	0.5	6	0.5	−5.2
290	0.5	6	−0.5	−1.6
303	1.5	6	−0.5	8.0
317	0.5	7	0.5	0.8
317	0.5	8	−0.5	6.0
362	0.5	8	−0.5	−2.4
362	0.5	8	0.5	−3.5
380	1.5	9	−0.5	−1.4
380	1.5	10	−0.5	−0.5
393	1.5	11	−0.5	2.5
412	1.5	12	−0.5	−3.5
421	0.5	11	−0.5	1.4
453	0.5	12	−0.5	−1.7
453	0.5	12	0.5	−0.4
457	1.5	13	−0.5	2.4
463	0.5	14	−0.5	4.1
469	1.5	14	−0.5	4.9
506	0.5	17	−0.5	−2.8
527	0.5	19	−0.5	3.8
546	1.5	19	−0.5	−8.4
555	1.5	20	−0.5	1.2
562	0.5	21	−0.5	2.5

TABLE IV. Comparison of the Jahn–Teller parameters[a] of the trichlorosiloxy and various methoxy free radicals.[b]

Parameter	$SiCl_3O$	CH_3O	CD_3O	CF_3O	CF_3S
$\omega''_{e,5}$	251.0	1417	1070	600	536
D_5	0.396	0.075	0.17	0.04	<0.01
K_5	−0.162	−0.032	−0.03	…	…
$\omega''_{e,6}$	152.5	1065	825	465	320
D_6	0.916	0.24	0.20	0.45	0.24
K_6	−0.048	−0.14	−0.16	0.05	…
$a\zeta_e$	−183	−145	−145	−140	−360
ε_{total}	239	419	410	233	77
ε^{SO}_{total}	203	370	367	203	0

[a] All quantities in cm^{-1} except for D and K which are dimensionless.

[b] Ref. 23.

is the measured vibrational energy relative to the lowest 0_0^- ($j = ½$) level, the j value, n_j, which an index identifying the n_jth eigenvalue of a given value of j and Σ, and Σ, the quantum number for the projection of the total electron spin angular momentum on the symmetry axis. In this case, for $j = ½$, $\Sigma = +0.5$ for the lower spin–orbit component and −0.5 for the upper spin–orbit component, whereas the $j = 3/2$ levels are not split by spin–orbit coupling, so only $\Sigma = -0.5$ levels were calculated. The energy levels to be fitted were only those involving the Jahn–Teller active modes ν_5 and ν_6; levels that contained one or more quanta of the totally symmetric vibrations were not included.

The parameters to be varied in fitting the data were the harmonic vibrational frequency $\omega_{e,i}$ of each Jahn–Teller active mode i, their linear and quadratic Jahn–Teller coupling constants D_i and K_i, and the global spin–orbit coupling constant $a\zeta_e$. The fitting process was laborious as only one or two levels could be added to the dataset at a time, and the SOCJT program took 1–3 h to execute on a 3.4 GHz central processing unit (CPU) desktop computer.

As shown in Fig. 2, absorption from the 0_0^- ($j = ½$) level can only populate $j' = 0$ (0^0, 1^1, 6^2, etc.) and $j' = 1$ levels (6^1, 5^1, etc.), which subsequently emit down to $j'' = ½$ or $j'' = ½$ and 3/2, respectively, severely limiting the range of observed levels in the ground state. As shown in Fig. 6, a few of the lowest levels [6_1^-, 6_1^+ ($j = 3/2$) and 5_1^-, 5_1^+ ($j = 3/2$)] were readily assigned and initially fitted. An examination of the eigenvector coefficients showed that the mixing was extreme, even for the very lowest levels, so that making vibrational assignments was generally not possible, and we had to resort to simply specifying the eigenvector with the quantum numbers j, n_j, and Σ.

Due to the substantial width of the emission features (7–10 cm^{-1}) and the broadening due to the various chlorine isotopologues, the transitions could not be measured to better than 1–2 cm^{-1}, so we have truncated the measured energy levels to the nearest wave number. For ground state energies up to about 300 cm^{-1}, the levels were fairly discrete and readily identified. Beyond that point, there were often multiple almost degenerate calculated energy levels, so the assignments were made on less secure grounds. We used three criteria for making assignments starting with the j value, where determinable, particularly for $j = 3/2$, which were identifiable by their absence from the 0^0 and 3^1 level emission spectra. Second, bootstrapping up from a minimal set of well-defined levels, there had to be a good correspondence between observed and calculated values. Third, there had to be reasonable agreement between the observed and calculated intensities in the various emission spectra. After each least squares refinement, we checked these criteria before augmenting the dataset. In the majority of the emission spectra, there are few strong transitions with displacements greater than 600 cm^{-1}, and assignments became very problematic beyond that point, due to the density of Jahn–Teller active levels and the extensive mixing of the basis states.

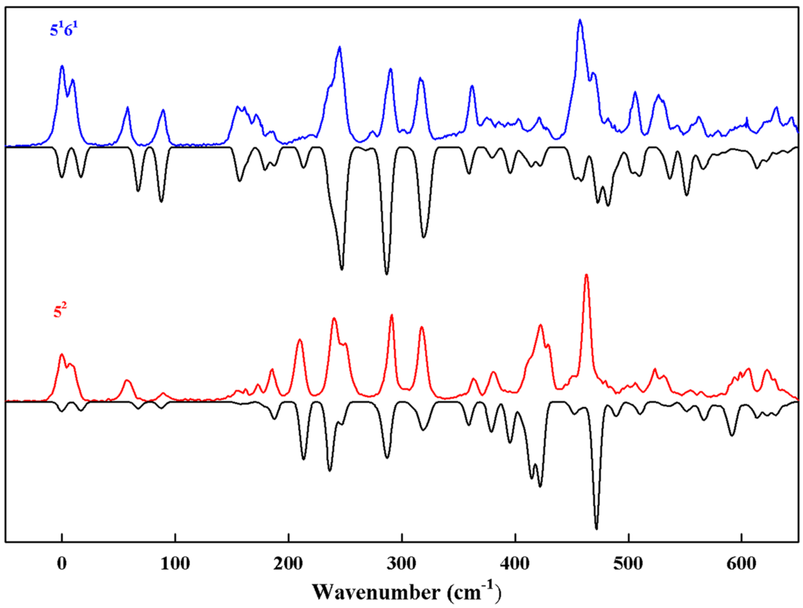

FIG. 7. A comparison of the experimental (upward going) and SOCJT simulated (downward going) single vibronic level emission spectra from the $5^1 6^1$ and 5^2 levels of the $SiCl_3O$ free radical. The spectra are plotted as displacement from the laser excitation wave number (cm^{-1}), giving a direct measure of the relative ground state energy for each transition.

In the final analysis, we fitted 35 ground state assignments, varying seven constants for an overall standard deviation of 4.0 cm^{-1}, with the results shown in Tables III and IV. Care was taken to ensure that the basis set was large enough to guarantee reasonable convergence. The agreement between the observed and calculated emission spectra for the higher $5^1 6^1$ and 5^2 levels, which provide a stringent test of the analysis, is illustrated in Fig. 7. Recalling that only activity in the Jahn–Teller modes, ν_5 and ν_6, is simulated and that the observed energy levels have residuals ranging up to almost 10 cm^{-1}, the agreement between the observed and calculated spectra is quite satisfactory.

IV. DISCUSSION

The results presented in this paper are the first detailed Jahn–Teller analysis of the electronic spectrum of a gas phase free radical as heavy as $SiCl_3O$. The presence of two low frequency Jahn–Teller active modes and the additional complication of the spin–orbit coupling make the spin-vibronic energy level structure in the ground state quite complex. Of the 29 levels involving ν_5'' and/or ν_6'' that we calculate in the first 400 cm^{-1}, we have assigned 22, or 76%. Possible transitions to the unassigned levels are overlapped by other transitions, either involving nondegenerate modes (such as ν_3'') or assigned features calculated to be more intense.

It is of interest to compare the Jahn–Teller effect in the trichlorosiloxy radical with that in the much better known methoxy radicals, as documented in Table IV. In all cases, the major Jahn–Teller active modes are ν_5'' and ν_6'', although there is a slight contribution from ν_4'' in CH_3O and CD_3O. The siloxy linear Jahn–Teller parameters D_i are much larger than those of the methoxy radicals, primarily due to the much smaller vibrational frequencies in the former. In the linear coupling approximation, the contribution of mode i to the depth of the moat relative to the symmetric configuration is $\varepsilon_i^{(1)} = D_i \omega_{e,i}$, so for a fixed $\varepsilon_i^{(1)}$, D_i increases as the vibrational frequency decreases. Indeed, the data at the bottom of Table IV shows that the total $SiCl_3O$ linear Jahn–Teller stabilization energy (239 cm^{-1}) is less that of CH_3O and CD_3O but comparable to that of CF_3O. In the present case, both modes make a sizable contribution to the linear Jahn–Teller stabilization energy, with $\varepsilon_5^{(1)} = 99$ cm^{-1} and $\varepsilon_6^{(1)} = 140$ cm^{-1}, whereas $\varepsilon_6^{(1)} = 209.3$ cm^{-1} clearly dominates in CF_3O. The significant contribution of both $SiCl_3O$ modes is evident in the LIF (Fig. 4) and emission (Fig. 6) spectra, where transitions involving ν_5 and ν_6 predominate.

Spin–orbit coupling competes with Jahn–Teller coupling for the electronic orbital angular momentum: they involve the coupling of the electronic orbital angular momentum of the molecule to either the spin angular momentum or the vibrational angular momentum, respectively. Barckholtz and Miller[8] discuss two separate regimes: one where the spin–orbit coupling largely eliminates the Jahn–Teller distortion (when $a\zeta_e > 4D_i\omega_{e,i}$) and the other where the molecule is distorted but the spin–orbit splitting is quenched (when $a\zeta_e < 4D_i\omega_{e,i}$). The former is exemplified in the ground state of the CF_3S radical, where the inclusion of the spin–orbit coupling drops the Jahn–Teller stabilization to 0 cm^{-1} ($|a\zeta_e| = 360$ cm^{-1} $> 4D_6\omega_{e,6} = 307$ cm^{-1}) and there is no geometric distortion. The latter regime is more typical as shown in Table IV, where the spin–orbit coupling only slightly diminishes the total Jahn–Teller stabilization, including a small 15% effect in $SiCl_3O$.

The measured splitting of the 6_1 ($j = 3/2$) levels (see Fig. 4 and Table III) is 31 cm^{-1}, much larger than the 10 cm^{-1} splitting of the 0_0 ($j = ½$) levels. As discussed elsewhere,[8] this enhanced splitting of the $j = 3/2$ levels is caused by the presence of quadratic coupling in the Jahn–Teller modes. In this case, the total quadratic Jahn–Teller stabilization energy $\varepsilon = D_5\omega_{e,5}K_5 + D_6\omega_{e,6}K_6 = 23$ cm^{-1}, about 10% of the linear contribution and rather smaller than the 39 cm^{-1} total quadratic stabilization in the methoxy free radical.[22] This implies that the minima and maxima around the $SiCl_3O$ moat are separated by only $2\varepsilon_{total}^{(2)} = 46$ cm^{-1}. We also note that our spectrum fits just as well with positive or negative starting values of the quadratic constants K_i, whereas the signs are predominantly negative in the methoxy radicals (see Table IV). The primary effect of the sign of K_i is to affect the positions of the local minima and maxima around the moat. In addition, quadratic coupling breaks the degeneracy of the $j = 3/2$ levels into their a_1 and a_2 components, and the sign of K_i affects the relative energies of these levels. The spin–orbit coupling does not further split these levels, but rather mixes them together and shifts them. The extent of such mixing can be gauged from the relative intensities of the spin–orbit components. In the present case, the spin–orbit coupling is substantial and mixes the a_1 and a_2 levels of the lowest $j = 3/2$ levels so thoroughly that the spin–orbit components (6_1^+ and 6_1^- or 5_1^+ and 5_1^-) have very similar intensities in the dispersed fluorescence spectra. Since the signs of the K_i are indeterminate in the $SiCl_3O$ spectrum, we have elected to make them negative in accord with the results for the various methoxy radicals.

A. Comparison with theoretical predictions

We can compare the *ab initio* results in Table I to our experimental findings, to get an idea of the utility of such modest calculations. For the excited state, we find that our LIF values for $\nu_1 = 912.6$, $\nu_3 = 237.3$, $\nu_5 = 292.7$, and $\nu_6 = 163.6$ cm^{-1} are all within 2% of the B3LYP values, with generally slightly higher MP2 frequencies. Certainly, these theoretical frequencies, particularly in conjunction with a FC simulation of the spectrum, can be used to distinct advantage to identify and assign the LIF spectrum. In this case, the FC simulation works because only the vibrational zero-point level in the ground state is involved and the excited state is nondegenerate. Although both are deficient by almost 1200 cm^{-1}, the B3LYP and MP2 electronic excitation energies nicely bracket the experimental T_0 value, providing further confirmation of the carrier of the spectrum.

In the ground state, the only nondegenerate fundamentals we have assigned are $\nu_1 = 894$ cm^{-1} (904/872 cm^{-1}) in the 0–0 band emission spectrum and $\nu_3 = 233$ cm^{-1} (245/223 cm^{-1}) in the 3_0^1 band emission spectrum. The *ab initio* values given in parentheses (see Table I) are in good accord with the experimental assignments. The averages of the calculated frequencies for $\nu_5 = 246$ cm^{-1} and $\nu_6 = 139$ cm^{-1} are also in good accord with the harmonic basis function frequencies $\omega_5 = 251.0$ and $\omega_6 = 152.5$ cm^{-1} obtained in our Jahn–Teller analysis of the emission spectra.

We can obtain a crude estimate[22] of the expected Jahn–Teller stabilization by comparing the ground state energy of $SiCl_3O$ constrained to C_{3v} symmetry with that obtained from the relaxed geometry given in Table I. The results are B3LYP = 260 cm^{-1} and MP2 = 157 cm^{-1}, both in general agreement with the fitted total linear stabilization energy of 239 cm^{-1}. Theory clearly shows that our analysis gives a Jahn–Teller stabilization which is quite reasonable.

V. CONCLUSIONS

The trichlorosiloxy free radical has now been conclusively identified and characterized in the gas phase. The jet-cooled $SiCl_3O$ species has been studied by LIF and resolved emission techniques, and it has been shown that there is a substantial Jahn–Teller effect in the ground state. Thirty-five ground state spin-vibronic levels have been fitted to an overall standard deviation of 4.0 cm^{-1} using a Jahn–Teller model that includes multimode activity in ν_5 and ν_6 and substantial spin–orbit coupling. The spin–orbit splittings in the lowest $j = 3/2$ levels are significantly larger than those of the 0_0 level, indicating the necessity of including both linear and quadratic Jahn–Teller couplings. The spin–orbit coupling only slightly diminishes the Jahn–Teller stabilization in the $SiCl_3O$ free radical, leading to pronounced activity in the ν_5'' and ν_6'' Jahn–Teller active modes in the LIF and single vibronic level emission spectra.

ACKNOWLEDGMENTS

The authors thank Dr. Gretchen Rothschopf for her support with various aspects of this work and Dr. Brandon Tackett for early explorations of the $SiCl_4 + O_2$ spectrum. They are grateful to Timothy Barckholtz and Terrance Codd for valuable advice concerning the SOCJT program. This research was funded by Ideal Vacuum Products.

REFERENCES

[1] F. Ojeda, A. Castro-García, C. Gómez-Aleixandre, and J. M. Albella, J. Mater. Res. **13**, 2308 (1998).
[2] M. R. Zachariah and W. Tsang, J. Phys. Chem. **99**, 5308 (1995).
[3] *Chemical Vapor Deposition. Principles and Applications*, edited by M. L. Hitchman and K. F. Jensen (Academic Press, London, 1993).
[4] M. Binnewies and K. Jug, Eur. J. Inorg. Chem. **2000**, 1127, and references therein.
[5] M. Junker, A. Wilkening, M. Binnewies, and H. Schnöckel, Eur. J. Inorg. Chem. **1999**, 1531.
[6] M. Junker and H. Schnöckel, J. Chem. Phys. **110**, 3769 (1999).
[7] V. M. Donnelly and A. Kornblit, J. Vac. Sci. Technol., A **31**, 050825 (2013).
[8] T. A. Barckholtz and T. A. Miller, Int. Rev. Phys. Chem. **17**, 435 (1998) and references therein.
[9] R. Srinivas, D. K. Boehme, D. Suelzle, and H. Schwarz, J. Phys. Chem. **95**, 9836 (1991).
[10] M. C. R. Symons, J. Chem. Soc., Dalton Trans. Inorg. Chem. **16**, 1568 (1976).
[11] H. Niki, P. D. Maker, C. M. Savage, L. P. Breitenbach, and M. D. Hurley, J. Phys. Chem. **89**, 3725 (1985).
[12] H. Harjanto, W. W. Harper, and D. J. Clouthier, J. Chem. Phys. **105**, 10189 (1996).
[13] W. W. Harper and D. J. Clouthier, J. Chem. Phys. **106**, 9461 (1997).
[14] D. L. Michalopoulos, M. E. Geusic, P. R. R. Langridge-Smith, and R. E. Smalley, J. Chem. Phys. **80**, 3556 (1984).
[15] M. J. Frisch, G. W. Trucks, H. B. Schlegel *et al.*, GAUSSIAN 09, Revision A.02, Gaussian, Inc., Wallingford, CT, 2009.
[16] A. D. Becke, J. Chem. Phys. **98**, 5648 (1993).
[17] C. Lee, W. Yang, and R. G. Parr, Phys. Rev. B **37**, 785 (1988).
[18] G. Herzberg, *Molecular Spectra and Molecular Structure III. Electronic Spectra and Electronic Structure of Polyatomic Molecules* (Van Nostrand, New York, 1966).
[19] T. A. Barckholtz and T. A. Miller, Program SOCJT downloaded from https://www.asc.ohio-state.edu/miller.104/molspect/goes/software/socjt/index.html.
[20] D. S. Yang, M. Z. Zgierski, A. Bérces, P. A. Hackett, P. N. Roy, A. Martinez, T. Carrington, Jr., D. R. Salahub, R. Fournier, T. Pang, and C. Chen, J. Chem. Phys. **105**, 10663 (1996).
[21] B. S. Tackett, Y. Li, D. J. Clouthier, K. L. Pacheco, G. A. Schick, and R. H. Judge, J. Chem. Phys. **125**, 114301 (2006).
[22] T. A. Barckholtz and T. A. Miller, J. Phys. Chem. A **103**, 2321 (1999).
[23] T. A. Barkholtz, M.-C. Yang, and T. A. Miller, Mol. Phys. **97**, 239 (1999).